THE HISTONE CHAPERONE SPN1 PRESERVES SUBNUCLEOSOMAL STRUCTURES AT PROMOTERS AND NUCLEOSOME POSITIONING IN OPEN READING FRAMES

AUTHORS

Andrew J. Tonsager[1], Alexis Zukowski[2], Catherine A. Radebaugh[1], Abigail Weirich[2], Laurie A. Stargell[1,*], Srinivas Ramachandran[2,3*]

[1]Department of Biochemistry and Molecular Biology, Colorado State University, Fort Collins, CO, 80523-1870, USA

[2]Department of Biochemistry and Molecular Genetics, [3]RNA Bioscience Initiative, University of Colorado School of Medicine, Aurora, CO, U80045, USA

*Correspondence: srinivas.ramachandran@cuanschutz.edu, laurie.stargell@colostate.edu

ABSTRACT

Spn1 is a multifunctional histone chaperone essential for life in eukaryotes. While previous work has elucidated regions of the protein important for its many interactions, it is unknown how these domains contribute to the maintenance of chromatin structure. Here, we employ digestion by micrococcal nuclease followed by single-stranded library preparation and sequencing (MNase-SSP) to characterize chromatin structure in yeast expressing wild-type or mutants of Spn1. We mapped nucleosome and subnucleosomal protections genome-wide, and surprisingly, we observed a genome-wide loss of subnucleosomal protection over nucleosome-depleted regions (NDRs) in the Spn1-K192N-containing strain, indicating critical functions of Spn1 in maintaining normal chromatin architecture in promoter regions. Additionally, alterations in nucleosome and hexasome positioning were observed in markedly different mutant Spn1 strains, demonstrating that multiple functions of Spn1 are required to maintain proper chromatin structure in open reading frames, particularly at higher expressed and longer genes. Taken together, our results reveal a previously unknown role of Spn1 in the maintenance of NDR architecture and deepen our understanding of Spn1-dependent chromatin maintenance over transcribed regions.

INTRODUCTION

Eukaryotes package their genomes by wrapping ~147 bp of DNA in about 1.7 superhelical turns around an octamer of histone proteins to form nucleosomes (1-3). This process occurs in a stepwise manner, as DNA initially wraps around a tetramer of histones H3–H4 to form a tetrasome, followed by sequential additions of two H2A-H2B dimers to form a hexasome, then a nucleosome (4). Tetrasome and hexasome subnucleosomal structures have been observed both *in vitro* (5) and *in vivo* (6) and represent stable intermediates in nucleosome assembly and disassembly. Nucleosomes regulate DNA access to many proteins that perform essential processes such as DNA replication (7, 8), repair (7, 9), recombination (10), and transcription. Nucleosomes regulate transcription in a variety of ways. Positioning of nucleosomes at promoters can hinder transcription initiation by preventing the binding of transcription factors (11, 12) while positioning of nucleosomes within coding regions can play an important role in preventing intragenic transcription initiation by reducing the accessibility of factors to intragenic initiation sites (13). Nucleosomes inhibit elongation of protein-coding genes, as they pose a significant barrier to RNA polymerase II (RNAPII) and reduce its transcription rate (14, 15). As a result, chromatin structure must be dynamic to allow for selective gene expression. An important class of proteins responsible for modifying chromatin structure are histone chaperones, which bind histones and facilitate histone deposition, exchange, or removal from chromatin, independent of ATP (16).

Spn1 is a multifunctional and essential histone chaperone that is highly conserved across eukaryotes. *S. cerevisiae* Spn1 preferentially binds H3-H4 histones (17) via its N-terminal region, with a high binding affinity (K_D ~ 10nM). Spn1 affinity to H3-H4 is at least 50-fold higher than that to H2A-H2B dimers (18). Spn1 can deposit H3-H4 onto DNA and facilitate the assembly of H3-H4 tetrasomes *in vitro* (17). Spn1 also has a well-characterized interaction with another essential histone chaperone Spt6; they bind each other with high affinity (K_D = 10-100nM) to form a heterodimer (19-22). The central domain of Spn1 is a highly conserved eight-helix bundle and is primarily responsible for binding Spt6 (18). Depletion of either protein through the auxin-

inducible degron system results in a reduction in recruitment of the other to chromatin (23). Spn1 binds nucleosomes with its C-terminal region (17, 18).

Cells with endogenous Spn1 replaced with the truncated *spn1*$^{141\text{-}305}$ mutant, lacking the N- and C-terminal domains described above, are viable (17, 24). However, Spn1$^{141\text{-}305}$ cannot bind nucleosomes and histones, though it retains the ability to bind Spt6 and RNAPII (17, 18). Yeast expressing *spn1*^{K192N} are also viable, and we have previously demonstrated that these cells have reduced Spn1 recruitment to the *CYC1* locus and fail to recruit Spt6 to *CYC1* (25). The *spn1*^{K192N} mutant also has reduced Spn1 binding to RNA Polymerase II (RNAPII) by co-immunoprecipitation (25). As recent work demonstrates that Iws1, the human ortholog of Spn1, serves as a hub that maintains association of numerous transcription elongation factors (26), it remains unclear which interactions are impaired that lead to loss of RNAPII recruitment.

While we and others have previously demonstrated that Spn1 possesses multiple interactions regarding chromatin functions, the role of Spn1 *in vivo* is not well understood. Here, micrococcal nuclease digestion followed by single-stranded library preparation and sequencing (MNase-SSP) (27) is used to characterize chromatin structure in yeast expressing wild-type or mutant Spn1 alleles. MNase-SSP allows for the analysis of nucleosomal, subnucleosomal and transcription factor protections genome-wide. We find that despite seemingly distinct functional defects, both *spn1*^{K192N} and *spn1*$^{141\text{-}305}$ expression show similar chromatin defects across genes, namely a progressive 3′ downstream shift in nucleosomes and intermediates over gene bodies. However, expression of *spn1*$^{141\text{-}305}$, but not *spn1*^{K192N}, produces a unique molecular mutant phenotype of a shift in the +1 and +2 nucleosome positions. Mapping the midpoints of the sequenced fragments reveals that shifts in nucleosomes and subnucleosomes occur as a downstream redistribution of occupancy at alternative rotational positions previously observed in the yeast genome (28). This molecular mutant phenotype of the shift downstream is largest at higher expressed and longer genes. Intriguingly, MNase-SSP also revealed a molecular mutant phenotype specific to cells expressing *spn1*^{K192N}: the loss of subnucleosomal protections over nucleosome-depleted regions (NDRs) in promoters. Taken together, these studies reveal the

importance of both the central domain of Spn1 and chromatin-binding disordered regions of Spn1 in preserving chromatin structure across the yeast genome.

MATERIAL AND METHODS

Yeast Culturing and Strains

All *Saccharomyces cerevisiae* strains were grown in yeast extract, peptone, and dextrose (YPD; 2% dextrose) media at 30°C. A description of yeast strains and plasmids is provided in Supplemental Table S1. The strains used in this study were previously created as described (17, 25, 29). In summary, strains were transformed with a covering plasmid expressing wild-type *SPN1* flanked by the *TOA1* promoter and terminator. Endogenous *SPN1* was replaced by a *LEU2* fragment flanked by the *SPN1* promoter and terminator through homologous recombination. Plasmids containing wild-type *SPN1*, $spn1^{K192N}$, or $spn1^{141\text{-}305}$ under the control of their native promoter and terminator were introduced into strains by plasmid shuffling.

Isolation of nuclei and Micrococcal nuclease digestion

Yeast nuclei isolation and MNase digestion were performed as described in (30) with modifications. Yeast strains were grown in 400 ml of YP +2% glucose until an OD_{600} of ~1.0 was reached. The cells were collected by centrifugation in a JA-10 rotor at 5,000 RPM for 10 minutes at 4°C. The supernatant was decanted from above the cell pellets, and the cells were suspended in 30 ml of Sorbitol buffer (50 mM Tris-Cl pH 7.5, 1.0 M Sorbitol, 10 mM $MgCl_2$, 10 mM 2-Mercaptoethanol and 1mM Phenylmethylsulfonyl fluoride (PMSF)). The cell suspensions were transferred to chilled 50 ml conical tubes and collected by centrifugation in a GPKR centrifuge at 3,200 RPM for 5 minutes at 4°C. The supernatants were decanted from above the cell pellets and the cells were washed two additional times with 30 mL of Sorbitol buffer. The mass of the cell pellets was determined, and the cells were suspended in 0.66 ml of Sorbitol buffer per gram of cells.

Spheroplasting was completed by adding 0.34 mL of Zymolase (10 $^{mg}/_{mL}$) per gram of cells and incubating at 30°C with gentle agitation until ~90% of the cells were converted to spheroplasts. The spheroplasts were collected by centrifugation in a GPKR centrifuge at 3,200 RPM for 5 minutes at 4°C and then gently washed two times with 5 ml of Sorbitol buffer as described above. The washed spheroplasts were suspended in 25 mL of Ficoll buffer (18% Ficoll 400, 20 mM Tris-Cl pH 7.5, and 0.5 mM $MgCl_2$), transferred to a 50 ml Potter-Elvehjem homogenizer and lysed on ice with six up-down even strokes with a handheld drill at max rpm. The lysates were transferred to chilled 25 ml centrifuge tubes, and the remaining cells were pelleted in a JA-20 rotor at 6400 x rpm for 5 minutes at 4°C. The supernatants containing yeast nuclei were transferred to new centrifuge tubes and pelleted at 15,000 x rpm at 4°C. The nuclei were suspended in 10 ml of MNase digestion buffer (20mM Tris-Cl pH 8.0, 1.5mM $CaCl_2$, 150mM NaCl, and 1mM PMSF). To estimate the yield of nuclei, 100 µl aliquots of the nuclei suspensions were diluted to 1 ml with MNase digestion buffer and the OD_{600} was determined. The nuclei were again pelleted at 15,000 x rpm for 30 minutes at 4°C and suspended in MNase digestion buffer at a ratio of 2.4 ml per 0.2 OD_{600}. Five aliquots (400 µl) of the nuclei suspensions were transferred to microcentrifuge tubes and incubated at 37°C for 10 minutes. Digestion buffer or MNase was added to samples to yield a final concentration of 0, 32, 64, or 128 U/ml, and incubation at 37°C continued for 10 minutes. 100 µl of stop solution (50mM EDTA, 2.5% SDS, 0.25mg/ml Proteinase K) was added to each reaction, and the samples were mixed and incubated at 37°C overnight. The MNase-digested DNA samples were extracted twice with phenol:chloroform, once with chloroform, and precipitated with ethanol. The DNA was washed with 70% ethanol, dried at room temperature, then suspended in 100 µl of TE buffer (pH 7.5) and 3 µl of RNaseA (10 mg/ml) added. The RNase reactions were incubated overnight at 37°C, followed by ethanol precipitation, washing with 70% ethanol, and drying at room temperature. The precipitated DNA samples were suspended in 100µl of TE buffer (10mM Tris-Cl, pH 8.0 and 1mM EDTA, pH 8.0), and 10µl of each sample was subjected to agarose gel electrophoresis.

Single-stranded DNA library preparation (SSP) and sequencing

MNase-protected DNA fragments were made into sequencing libraries using the single-stranded library protocol as previously described (27, 31, 32). In brief, 10ng DNA was dephosphorylated using FastAP Thermosensitive Alkaline Phosphatase (Thermo Scientific cat. EF0651), denatured, and incubated overnight with CircLigaseII (Lucigen cat. CL9025K) and 0.093-0.125 μM biotinylated CL78 primer (31) at 60ºC with shaking every 5 minutes. DNA fragments were then denatured and bound to magnetic streptavidin M-280 beads (Invitrogen cat. 11205D) for 30 minutes at room temperature with nutation. Beads were washed, and second-strand synthesis was performed using Bst 2.0 DNA polymerase (NEB cat. M0537) with an increasing temperature gradient of 15-31ºC with shaking at 1750 rpm. Beads were washed, and a 3' gap fill was performed using T4 DNA polymerase (Thermo Scientific cat. EL0011) for 30 minutes at room temperature. Beads were washed, and a double-stranded adapter was ligated using T4 DNA ligase (Thermo Scientific cat. EP0062) for 2 hours at room temperature with shaking at 1750 rpm. Beads were washed and resuspended in 30 μL 10 mM TET buffer (10 mM Tris-HCl pH 8.0, 1 mM EDTA pH 8.0, 0.05% Tween-20). DNA was denatured at 95ºC for 3 min, and DNA libraries were collected after immediate magnetic separation.

Quantitative real-time PCR was performed on DNA libraries using iTAQ Supermix (Bio-Rad cat. 1725124), and Ct values were used to determine the number of PCR cycles needed to amplify each library. PCR was performed with KAPA HiFi DNA polymerase (Kapa Biosystems cat. KK2502) using barcoded indexing primers for Illumina. Primer dimers were removed from the libraries using AMPure beads (Beckman Coulter cat. A63881). Libraries were eluted in 0.1X TE and concentrations were determined using Qubit. The length distribution of each library was assessed by the Agilent Bioanalyzer using the D1000 or HSD1000 cassette. Libraries were sequenced for 150 cycles in paired-end mode on the NovaSeq 6000 system at the University of Colorado Cancer Center Genomics Shared Resource.

MNase-SSP analysis

Sequencing reads were trimmed using Cutadapt (33): Illumina adapter sequences were removed, and reads were trimmed to 140 bp. Reads less than 35 bp were discarded. Trimmed reads were aligned to the sacCer3 version of *Saccharomyces cerevisiae* genome using bowtie2 (34).

Samtools (35) and bedtools (36) were used for processing aligned reads from sam to bed files. Coverage at 1 bp windows genome-wide for specific fragment lengths was calculated as the number of reads that mapped at each window, normalized by the factor N: N = 139712364/(Total number of mapped reads). 139712364 was a number chosen arbitrarily. Coverage of fragment centers for specific fragment lengths was also calculated similarly at 1 bp windows. V-plots were generated using custom scripts that are publicly available (https://github.com/srinivasramachandran/VPLOTS/). Nucleosome positions were obtained from (28). Transcription start sites were obtained from (37). Genes were stratified by expression using published NET-seq data (38). NET-seq normalized read counts were summed between TSS+100 and TSS+200.

RESULTS

MNase-SSP interrogates nucleosomal and subnucleosomal structures across the yeast genome

To study the role of Spn1 in maintaining chromatin structure, wild-type Spn1, *spn1*^{K192N}, and *spn1*$^{141-305}$ containing strains were subjected to MNase-SSP. MNase-SSP was performed with increasing levels of MNase, which digests linker DNA at 25 times the rate of nucleosomal DNA and produces protected genomic fragments of varied sizes (39). Samples were subjected to agarose gel electrophoresis to qualitatively assess the population of polynucleosomal, nucleosomal, and smaller fragment sizes after MNase digestion (**Supplemental Fig. S1A**). Fragments of all lengths were sequenced and mapped to the *S. cerevisiae* genome. To map nucleosome and subnucleosome positioning in WT and Spn1 mutants, a metagene analysis was performed to generate plots of fragment midpoint versus fragment length ("V-plots") (11) centered at the dyad of each nucleosome downstream of the transcription start site from the +1 to +10 positions. To construct V-plots, we randomly sampled fragments genome-wide to yield similar fragment length distributions across WT and Spn1 mutant datasets (**Supplemental Fig. S1B**). Dyad definitions from chemical cleavage mapping were used to define nucleosome dyad positions spanning 4688 yeast genes (28) (**Supplemental Fig. S2**). The density at position 0 and

fragment length 147 bp corresponds to the strongest dyad signal in chemical cleavage mapping. V-plots centered at +1, +2, and +5 exemplify that plots at each nucleosome position show a checkered pattern that appears similar across both wild-type and mutant samples (**Figure 1A**). At nucleosomal size fragments (~150 bp), this arises from peaks in density separated by a 10 bp periodicity on either side of the dyad, corresponding to nucleosome occupancy at previously mapped rotational positions surrounding yeast nucleosomes (28, 40). The V-plots reveal the existence of rotational positioning of subnucleosomal structures in all the samples.

While the V-plots provide an extensive picture of chromatin protections of varying sizes across the yeast genome, it is difficult to make comparisons between datasets from wild-type and mutant Spn1 strains. To analyze the change in the chromatin landscape in mutant Spn1 expressing yeast compared to wild-type yeast, we generated difference V-plots by subtracting mutant V-plots from wild-type (**Supplemental Fig. S3**). The *spn1*^{K192N} mutation, but not *spn1*$^{141-305}$, produces a loss in short fragments 50-150 bp upstream of the +1 dyad, corresponding to a decrease in protection over nucleosome-depleted regions (NDR) (**Figure 1B**). In contrast, the expression of *spn1*$^{141-305}$ produces a pattern of fragment loss directly over the +1 dyad with a corresponding increase in fragments immediately downstream. This shift in fragment distribution is consistent across fragment lengths 50-150 bp, corresponding to shifts in both nucleosomal and subnucleosomal protections. The pattern of a decrease in fragment density over the dyad and a corresponding increase downstream is observed at subsequent downstream dyad positions in both *spn1*$^{141-305}$ and *spn1*^{K192N} (**Figure 1B**). These results reveal that both the central and unstructured N- and C-terminal regions of Spn1 have overlapping roles in maintaining chromatin structure over genes but with functional differences proximal to transcription start sites.

Spn1 is required for accurate nucleosome positioning particularly at higher expressed and longer genes.

The previous figure showed V-plots generated by summing mapped fragment occupancy over all genes. To further the analysis from average changes to those of individual genes, the

normalized counts of 80-170bp fragments were plotted as a heatmap (**Supplemental Fig. S4A**). Genes were aligned by their +1-nucleosome dyad position and ranked by length. To determine if wild-type and mutant strains possess different patterns, the wild-type occupancy scores were subtracted from the *spn1*^{K192N} or *spn1*$^{141-305}$ samples to generate a difference heatmap (**Figure 2A**). Strikingly, this analysis reveals that loss of protection across NDRs in the *spn1*^{K192N} mutant is pervasive across the yeast genome (**Figure 2A,** left panel). Additionally, the difference heatmap reveals a striated pattern across the open reading frames of genes in both mutants, indicating a downstream shift in nucleosome positioning. This result aligns with the metagene analysis performed using the V-plots and additionally demonstrates that the defects observed in the V-plots occur consistently across genes throughout the genome. The fragment size bin used for the difference heatmap is sufficiently wide (80-170 bp) that it includes fragments protected by subnucleosomes (6). To specifically assess changes in nucleosome protections in the Spn1 mutant expressing strains, we repeated our analysis by exclusively mapping 142-152 bp fragments over our gene list. We observe a striated pattern in the difference heatmap over open reading frames similar to the pattern observed in the difference heatmap generated with 80-170bp fragments. However, the loss of protection in the NDR previously seen in *spn1*^{K192N} cells is not present in this fragment size bin (**Supplemental Fig. S4B**, **S4C**), indicating nucleosome protections are unchanged in the NDR.

To investigate nucleosome positioning across gene bodies further, an additional metagene analysis was performed by averaging the normalized read count over genes and plotting the result as a profile. The wild-type strain produces the expected profile of regularly phased and well-positioned nucleosomes (**Figure 2B**). As expected, nucleosome positions become "fuzzier" with each downstream nucleosome from the TSS; increases in the variability of distance of downstream nucleosome positions from the TSS result in a wider and flatter peak within the population. This analysis reveals that expression of both *spn1*^{K192N} and *spn1*$^{141-305}$ mutant alleles produced a progressive 3' downstream shift in nucleosome positioning, despite the known functional differences in *spn1*^{K192N} and *spn1*$^{141-305}$. To further examine differences between the wild-type and mutant nucleosome profiles, the difference in reads was quantified between wild-type and mutant samples and plotted alongside the wild-type nucleosome density (**Figure 2C**).

This difference plot demonstrates that while nucleosome protections shift in both mutant strains, nucleosome positions +1 and +2 shift specifically in cells expressing the *spn1*$^{141-305}$ allele. This result reveals that Spn1 maintains nucleosome positioning across genes, but the contributions of its functional domains differ in the maintenance of nucleosomes at the 5′ ends of genes versus across gene bodies.

As Spn1 is part of the RNAPII elongation complex, defects in chromatin structure observed in Spn1 mutant strains may be largest at the most highly transcribed genes, especially since Spn1 occupancy over coding genes is highly correlated to RNAPII occupancy (Rpb1) over those genes (23, 41, 42). To test this hypothesis, genes were first ranked by Rpb3 occupancy (a subunit of RNAPII) using published NET-seq data (38). Across all quartiles, the number of genes with nucleosomes positioned at +1 through +10 was relatively consistent (**Supplemental Fig. S5A**). Mapping the sequenced fragments 80-170 bp in length over each set of genes demonstrated that the highest quartile of genes ranked by expression exhibited larger shifts compared to the average gene in both *spn1*^{K192N} and *spn1*$^{141-305}$ expressing yeast (**Figure 2D, Supplemental Fig. S5B**). In contrast, genes in the lowest quartile of expression experienced a slightly lesser shift in nucleosome positioning compared to the average gene.

The expression of *spn1*$^{141-305}$, but not *spn1*^{K192N}, produces a shift in the +1 and +2 nucleosome positions (**Figure 2C**). This reveals that the maintenance of promoter-proximal nucleosomes (+1 and +2) and promoter distal nucleosomes (+3 to +10) may be functionally distinct. Genes across the yeast genome vary in length, and this prompted an investigation of gene length as a parameter for nucleosome shift. To begin examining this relationship, the gene list was ranked by length into quartiles of equal gene numbers (**Supplemental Fig. S6A**). Mapping the sequenced fragments 80-170 bp in length over each set of genes demonstrated that the furthest downstream nucleosomes present in the longest quartile of genes exhibit the largest shift in nucleosome position (**Figure 2E, Supplemental Fig. S6B**). Strikingly, the set of shortest genes experienced, on average, minimal defects in nucleosome positioning, even at nucleosome positions that were shifted in the longer genes. To verify these changes in chromatin protections are present specifically in nucleosomes, and that the results are not driven exclusively by smaller

subnucleosomal protections, the analysis was repeated with the 142-152 bp fragments. We observed a similar positive correlation between the extent of nucleosome positioning shift and both gene expression and gene length (**Supplemental Figs. S7, S8**). Taken together, these results suggest that Spn1 maintenance of chromatin structure becomes increasingly critical at highly expressed and longer genes.

The *spn1^{K192N}* mutation reduces stability over nucleosome-depleted regions

The MNase-SSP results demonstrate that expression of either *spn1^{K192N}* or *spn1$^{141-305}$* generates a downstream shift in chromatin protections over yeast open reading frames. In contrast, a loss in MNase-protected fragments in the nucleosome-depleted regions (NDRs) was observed specifically in the *spn1^{K192N}* mutant yeast strain (**Figure 1A, B**). Our further analysis demonstrated that this loss is present in the 80-170 bp fragments. However, the 142-152 bp fragments were not responsible for the loss of this range of protected fragments coming from NDRs. As previously stated, this bin of fragments is sufficiently wide that it contains protection by subnucleosomes. More specifically, the abundance of protected fragments both 83-93 bp and 102-112 bp in size can be interpreted as DNA bound by hexasomes (6). To test if *spn1^{K192N}* cells exhibit loss in protected fragments 83-93bp and 102-112bp in size over the NDR, we analyzed the enrichment of these fragments, revealing a loss in hexasomal protections over the NDR (**Supplemental Fig. S9**). This result indicates that the loss in 80-170 bp fragment protection observed in *spn1^{K192N}* is at least in part driven by a loss in hexasome protection.

NDRs are flanked by well-positioned -1 and +1 nucleosomes, which reside directly upstream and downstream of this region. Chromatin remodelers, such as the RSC complex, actively maintain NDRs after nucleosome deposition (43). This region is bound by many other factors, such as activators and enhancers that bind and compete with nucleosome formation within NDRs, contributing to the low nucleosome density in these regions (44). Nucleosome-depleted regions upstream of transcription start sites contain promoter sequences bound by transcription initiation factors. Overall, NDRs are protected by a variety of factors, many of which have smaller footprints (<60 bp). To explore if *spn1^{K192N}* cells have reduced protection in these smaller footprints over NDRs, we analyzed the enrichment of short (<60 bp) fragments, revealing a

dramatic loss in fragments in this strain over NDRs (**Figure 3A**). As our prior analysis demonstrated that hexasome protection in the NDR was reduced in *spn1*^{K192N} cells, this prompted the question of if tetrasome protection is also reduced in NDRs. The abundance of tetrasomes can be interpreted by mapping fragments 61-71 bp in length as previously shown (6). Analyzing the enrichment of fragments 61-71 bp in length revealed a similar dramatic loss in fragments in *spn1*^{K192N} over NDRs (**Figure 3B**). These results demonstrate that hexasomes, tetrasomes, and other smaller protections are lost in NDRs in *spn1*^{K192N} cells, with the loss becoming increasingly dramatic as fragment length decreases.

NDRs are maintained and protected by a wide range of proteins, including those sensitive to MNase (11, 12, 39). By varying MNase concentration, less stable structures can be revealed that are more sensitive to higher levels of MNase. To probe the MNase sensitivity of the NDR in Spn1 mutants, nuclei were digested with a low amount of MNase and we mapped smaller fragments from these samples to find that the NDR is largely unaffected (**Figure 3C, D**). This demonstrates that *spn1*^{K192N} cells exhibit a defect in NDRs, which renders them significantly less stable than in wild-type cells at higher MNase concentrations. Taken together, this indicates that the stability of the NDR is compromised in *spn1*^{K192N} cells, as shown by a reduction in protection when digested with a high concentration of MNase.

Quantification of nucleosome positioning shifts reveals that nucleosomal rotational position preference is redistributed in Spn1-mutant cells

Our analysis of the MNase-SSP data from wild-type and mutant Spn1 expressing yeast thus far has revealed global changes in nucleosome positioning across open reading frames genome-wide. An important characteristic of the data featured in the V-plots is the ability to capture alternate rotational positions occupied by nucleosomes around their mapped dyad locations (**Figure 1**). These positions correspond to DNA sequences with favorable histone-DNA interactions (45, 46). Based on the preservation of rotational positions in the Spn1 mutants observed in the V-plots, we hypothesized that nucleosome positioning shifts would occur in discrete steps at alternative, favorable DNA sequences in the mutants. To test this, the changes in density of 142-152 bp fragment midpoints were mapped relative to each nucleosome

position downstream of the TSS individually. The results of this analysis are consistent with the prior results that shifts in nucleosome positioning occur most dramatically at downstream nucleosome positions in more highly expressed and longer genes (**Figure 4A, B; Supplemental Figs. S10, S11**). Notably, the analysis also reveals that shifted nucleosomes occupy the same rotational positions as wild-type cells but with higher occupancy at rotational positions downstream of the dyad with a loss of occupancy at positions upstream of the dyad location (**Figure 4A, B; Supplemental Figs. S10, S11**).

As the shift in nucleosomes manifests as a change in nucleosome occupancy at discrete nucleosome positions, nucleosome positioning shift can be quantified by calculating the change in occupancy at each rotational position at each nucleosome. To accomplish this, the Z-scores across -5 to +5 rotational positions were calculated for each mapped nucleosome dyad for each gene. A positive Z-score denotes a preferred rotational position within a nucleosome position. The Z-scores of wild-type Spn1 were subtracted from the Z-scores of Spn1 mutants to obtain changes in rotation position preference due to Spn1 mutation. The median difference in Z-scores was plotted across all genes at each rotational position of each nucleosome position. The previous analysis indicates that the shifts in nucleosome positioning were correlated with gene expression and gene length. To evaluate the extent to which these correlations are significant, Z-scores and p-values (using the Wilcoxon Rank Sum test) were calculated for the changes in fragment midpoint occupancy at each rotational position around each nucleosome dyad for the genes in our previously determined quartiles of expression and length. This revealed that the number of rotational positions with significant changes in nucleosome occupancy increases with gene expression and length for both Spn1 mutant-expressing cells (**Figure 4C, D**). Additionally, *spn1*$^{141\text{-}305}$ mutant cells exclusively have rotational positions with significant changes in nucleosome occupancy at the +1 and +2 nucleosome positions. This demonstrates that the disordered N- and C-terminal regions of Spn1 specifically play a role in the proper maintenance of nucleosomes at the 5′ end of open reading frames. While both mutant strains experience shifts in nucleosome positions, *spn1*$^{141\text{-}305}$ mutant cells exhibit more positions with significant changes in nucleosome occupancy over open reading frames. These results support the model

that Spn1 preserves nucleosome positioning over genes, and this function becomes increasingly critical at higher expressed and longer genes.

Subnucleosomal intermediates are mispositioned in Spn1 mutant strains

An advantage to the MNase-SSP approach is the retention of small fragments in MNase-digested samples (**Supplemental Fig. S1B**), which can be mapped to the genome to determine the occupancy and positioning of subnucleosomal intermediates (6, 11). As previously mentioned, the abundance of protected fragments 102-112 bp in size can be interpreted as DNA bound by hexasomes (6). As hexasomes are a subnucleosomal intermediate produced during transcription, Spn1 mutation may also generate mispositioned hexasomes. To test this hypothesis, the midpoints of protected fragments 102-112 bp in size were mapped over 1st and 4th quartiles of genes ranked by expression or length. As was observed in the V-plots, plotting the midpoints of these fragments demonstrates the existence of alternative hexasome rotational positions around mapped nucleosome dyad positions with 10 bp periodicity on either side of the dyad (**Figure 5A, B; Supplemental Figs. S12, S13**). In contrast to nucleosome-protected fragments, the relative occupancy of hexasome protection is distributed more equally across the rotational positions upstream and downstream of the dyad position, most probably due to the fact that loss of contacts to an H2A-H2B dimer shifts the location of the midpoint on the DNA protected by a hexasome (6). As transcription through nucleosomes generates hexasomes with transient loss of contacts to both proximal and distal H2A-H2B dimers, the protected fragments have midpoints shifted on either side of the dyad that result in a wider distribution of hexasome-occupied rotational positions. Both Spn1 mutants exhibited a length- and expression-dependent downstream shift in rotational positioning preference of hexasomal protections (**Figure 5A, B; Supplemental Figs. S12, S13**).

To quantify and statistically validate the shifts observed in *spn1*^{K192N} and *spn1*$^{141-305}$ cells, Z-scores and p-values were calculated at rotational positions around each mapped dyad location as described before with gene lists ranked by expression and length (**Figure 5C, D**). This demonstrated that mutation of Spn1 produces a similar trend to the one found with nucleosome positioning, where hexasomes are redistributed from upstream rotational positions

to downstream positions in both *spn1*^{K192N} and *spn1*$^{141-305}$ cells. As seen before, more positions had significant changes in occupancy in *spn1*$^{141-305}$ cells than *spn1*^{K192N}, including shifts at the +1 and +2 dyad locations seen exclusively in *spn1*$^{141-305}$ cells, with more positions experiencing significant changes in hexasome occupancy at higher expressed and longer genes (**Figure 5C, D**).

Loss of both H2A-H2B dimers produces tetrasomes, and their genome-wide occupancy and positioning can be interpreted by mapping protected fragments 61-71 bp in length over the yeast genome, as previously stated (6). For 61-71 bp fragments, rotational positions were even more equally distributed compared to hexasomes due to the larger shifts in their midpoints compared to nucleosomal fragments (**Figure 6A, B; Supplemental Figs. S14, S15**). Tetrasomal protections in *spn1*^{K192N} have minimal changes compared to wild-type, even at highly expressed genes or longer genes. However, tetrasomal protections in *spn1*$^{141-305}$ show significant shifts to downstream rotational positions (similar to hexasomes) as a function of length and expression (**Figure 6C, D**). In summary, *spn1*$^{141-305}$ but not *spn1*^{K192N} results in significant shifts in tetrasomal rotational position preferences as a function of length and expression.

DISCUSSION

In this study, an extensive mapping of chromatin protections in yeast expressing functionally distinct mutant alleles of Spn1 was performed to assess the role of this essential histone chaperone in maintaining chromatin structure. By retaining fragments of a wide range of sizes, the MNase-SSP approach demonstrates that Spn1 preserves both nucleosomal and subnucleosomal protections across the yeast genome. Our analyses revealed that this function of Spn1 is critical for maintaining chromatin over NDRs, the 5′ ends of genes, and within gene bodies, through potentially distinct mechanisms.

The role of Spn1 in the maintenance of NDR architecture was previously unknown. While chromatin defects in Spn1 mutants have been primarily characterized over gene bodies during transcription elongation (23, 41), the *spn1*^{K192N} mutation clearly reduces subnucleosomal

structures in the NDR. The mechanism by which this mutation leads to this defect remains unclear. The *spn1*^{K192N} mutant is defective for recruitment to the RNAPII elongation complex, likely in part through disruption of interactions with Spt5 and Spt6 (25, 47). Most investigations of Spn1 and its interactions are primarily focused on its role as an elongation factor over gene bodies. For example, previous work with mutants that disrupt the Spn1-Spt6 complex has implicated the complex in monitoring nucleosomes over genes, and weakening the Spn1-Spt6 interaction has impacts on the assembly and maintenance of chromatin (41, 48). Additionally, compromise of Spt6 function has been shown to produce aberrations in chromatin over gene bodies, namely the misincorporation of histone variant H2A.Z (49). Our findings support the notion that surveillance of proper chromatin structure by the Spn1-Spt6 complex may extend to the NDRs.

Both *spn1*^{K192N} and *spn1*$^{141-305}$ produced a downstream shift in nucleosome positioning over gene bodies. However, *spn1*$^{141-305}$ exclusively exhibited defects in the positioning of the +1 and +2 nucleosomes. This finding reveals that the mechanism of chromatin maintenance at the 5′ ends of genes may be functionally distinct from that over the rest of the gene and that the histone- and nucleosome-binding functions of Spn1 are part of this mechanism. As *spn1*^{K192N} did not produce significant shifts in nucleosome or subnucleosome positioning at the 5′ ends of genes, one possible interpretation is that the mechanism of chromatin maintenance at the promoter-proximal region of genes requires Spn1 to directly bind chromatin, whose binding regions are unaffected in *spn1*^{K192N}. In contrast, maintenance of chromatin over the rest of the body of the gene requires both Spn1 recruitment to the RNAPII complex and its histone- and nucleosome-binding capabilities, as evidenced by defects in nucleosome and subnucleosome positioning at nucleosomes distal from the promoter in both mutants.

The requirement for Spn1 in preserving nucleosome positioning shares features with the functional requirements for Spt4 and Spt6 in maintaining chromatin structure (41, 50). Each of these factors are physically associated with RNAPII during transcription elongation, with Spn1 and Spt4 positioned at the tip of the RNAPII clamp facing the downstream DNA (47). In contrast, while the Spt6 N-terminal helices that bind Spn1 are also proximal to the downstream DNA, the

main body of Spt6 is docked near the upstream DNA exit channel (47). Spt6 binds histones and nucleosomes when the HMG-box-like protein Nhp6 is present (48). Spt6 is commonly attributed as a histone chaperone necessary for nucleosome reassembly in the wake of RNAPII, supported by its proximity to upstream DNA and its ascribed ability to suppress intragenic transcription (13, 51, 52). While Spt4 has not been shown to bind chromatin, it oscillates on and off RNAPII along with its binding partner Spt5 based on nucleosome positions, and its deletion produces a downstream nucleosome positioning shift. Moreover, Spt5 deletion produces increased stalling and backtracking during early transcription elongation (50). Despite differences in their transcription-associated functions, Spn1, Spt4, and Spt5 are all critical for maintaining proper chromatin structure, and strikingly, defects in each produced a similar pattern of downstream shifts in nucleosome positioning. One explanation for this commonality is that all participate in this process of co-transcriptional nucleosome disassembly and reassembly, and a defect in any step of this process might produce a similar defect in chromatin. Others have posed that this defect in passage through nucleosomes may produce an elongation complex that transcribes through chromatin more slowly than in wild-type cells, which might produce mispositioned nucleosomes (50). Indeed, there is evidence that loss of RNAPII transcription shifts nucleosome positions, as depletion of Rpb1 (53) and growth of the temperature-sensitive *rpb1-1* allele at a non-permissive temperature (54) produces a downstream nucleosome shift.

By mapping the fragment midpoints, we utilized our dataset to demonstrate that shifts in nucleosome positioning in Spn1 mutants occur in discrete steps at alternate favored rotational positions. Quantifying the occupancy of nucleosomes at each rotational position is an alternative method for statistically validating shifts in nucleosome positioning. This approach in quantifying shifts in nucleosome positions may be useful for other datasets of sufficiently high sequencing depth in organisms with small genomes like *S. cerevisiae*. The mapping of smaller fragments protected by subnucleosomal intermediates also demonstrated *in vivo* evidence of alternate rotational positions occupied by hexasomes and subnucleosomes. These positions also occurred in discrete steps of 10 bp on either side of the dyad, and hexasome and tetrasome occupancy were distributed more evenly across the positions surrounding the mapped nucleosome dyad position.

A puzzling question that remains is how *spn1*^{K192N} and *spn1*$^{141\text{-}305}$ produce such similar changes in nucleosome and hexasome positioning over nucleosomes distal to promoters despite their vast functional differences. Both Spn1 recruitment to the elongating RNAPII complex and its ability to bind histones and/or nucleosomes are critical for preserving chromatin structure, and likely occur co-transcriptionally. Wild-type Spn1 is poised near the downstream nucleosome in the RNAPII elongation complex (47). Spn1 directly binds histones and nucleosomes, a function that may be important for the disassembly of downstream nucleosomes during transcription. If the recruitment of Spn1 to sites of transcription is diminished, the process of disassembling the downstream nucleosome may be impacted. Conversely, the *spn1*$^{141\text{-}305}$ mutant is likely still recruited to sites of transcription. However, its loss of histone- and nucleosome-binding regions renders it unable to participate in the process of downstream nucleosome disassembly. In either mutant, the loss of Spn1 function results in defects in chromatin preservation during transcription elongation, resulting in a shift in nucleosome and hexasome positioning. Taken together, these findings deepen our understanding of Spn1-dependent chromatin maintenance over the yeast genome and provide insight into mechanisms underlying this process.

AUTHOR CONTRIBUTIONS

Andrew J. Tonsager: Conceptualization, Formal analysis, Investigation, Methodology, Visualization, Writing—original draft. **Alexis Zukowski**: Formal analysis, Methodology, Investigation. **Catherine A. Radebaugh**: Conceptualization, Formal analysis, Investigation, Methodology, Visualization. **Abigail Weirich**: Investigation. **Laurie A. Stargell**: Conceptualization, Funding Acquisition, Project administration, Supervision, Writing—review & editing. **Srinivas Ramachandran**: Conceptualization, Formal analysis, Funding Acquisition, Investigation, Methodology, Project administration, Supervision, Visualization, Writing—review & editing.

FUNDING

This work was supported by the RNA Bioscience Initiative, the University of Colorado School of Medicine, and NIH grant R35GM133434. S. R. is a Pew-Stewart Scholar for Cancer Research, supported by the Pew Charitable Trusts and the Alexander and Margaret Stewart Trust.

CONFLICT OF INTEREST

The authors declare that they have no known competing financial interests or connections, direct or indirect, that could have appeared to influence the work reported in this paper.

ACKNOWLEDGEMENTS

We thank Sarah Swygert for her expert technical assistance.

REFERENCES

1. Davey CA, Sargent DF, Luger K, Maeder AW, Richmond TJ. Solvent mediated interactions in the structure of the nucleosome core particle at 1.9 a resolution. J Mol Biol. 2002;319(5):1097-113.
2. Flaus A, Luger K, Tan S, Richmond TJ. Mapping nucleosome position at single base-pair resolution by using site-directed hydroxyl radicals. Proc Natl Acad Sci U S A. 1996;93(4):1370-5.
3. Luger K, Mader AW, Richmond RK, Sargent DF, Richmond TJ. Crystal structure of the nucleosome core particle at 2.8 A resolution. Nature. 1997;389(6648):251-60.
4. Polo SE, Almouzni G. Chromatin assembly: a basic recipe with various flavours. Curr Opin Genet Dev. 2006;16(2):104-11.
5. Brower-Toland BD, Smith CL, Yeh RC, Lis JT, Peterson CL, Wang MD. Mechanical disruption of individual nucleosomes reveals a reversible multistage release of DNA. Proc Natl Acad Sci U S A. 2002;99(4):1960-5.
6. Ramachandran S, Ahmad K, Henikoff S. Transcription and Remodeling Produce Asymmetrically Unwrapped Nucleosomal Intermediates. Mol Cell. 2017;68(6):1038-53 e4.
7. Groth A, Rocha W, Verreault A, Almouzni G. Chromatin challenges during DNA replication and repair. Cell. 2007;128(4):721-33.
8. Eaton ML, Galani K, Kang S, Bell SP, MacAlpine DM. Conserved nucleosome positioning defines replication origins. Genes Dev. 2010;24(8):748-53.

9. Adkins NL, Niu H, Sung P, Peterson CL. Nucleosome dynamics regulates DNA processing. Nat Struct Mol Biol. 2013;20(7):836-42.
10. Bevington S, Boyes J. Transcription-coupled eviction of histones H2A/H2B governs V(D)J recombination. EMBO J. 2013;32(10):1381-92.
11. Henikoff JG, Belsky JA, Krassovsky K, MacAlpine DM, Henikoff S. Epigenome characterization at single base-pair resolution. Proc Natl Acad Sci U S A. 2011;108(45):18318-23.
12. Kubik S, Bruzzone MJ, Jacquet P, Falcone JL, Rougemont J, Shore D. Nucleosome Stability Distinguishes Two Different Promoter Types at All Protein-Coding Genes in Yeast. Mol Cell. 2015;60(3):422-34.
13. Kaplan CD, Laprade L, Winston F. Transcription elongation factors repress transcription initiation from cryptic sites. Science. 2003;301(5636):1096-9.
14. Selth LA, Sigurdsson S, Svejstrup JQ. Transcript Elongation by RNA Polymerase II. Annu Rev Biochem. 2010;79:271-93.
15. Brahma S, Henikoff S. Epigenome Regulation by Dynamic Nucleosome Unwrapping. Trends Biochem Sci. 2020;45(1):13-26.
16. Bai L, Morozov AV. Gene regulation by nucleosome positioning. Trends Genet. 2010;26(11):476-83.
17. Li S, Almeida AR, Radebaugh CA, Zhang L, Chen X, Huang L, et al. The elongation factor Spn1 is a multi-functional chromatin binding protein. Nucleic Acids Res. 2018;46(5):2321-34.
18. Li S, Edwards G, Radebaugh CA, Luger K, Stargell LA. Spn1 and Its Dynamic Interactions with Spt6, Histones and Nucleosomes. J Mol Biol. 2022;434(13):167630.
19. McDonald SM, Close D, Xin H, Formosa T, Hill CP. Structure and biological importance of the Spn1-Spt6 interaction, and its regulatory role in nucleosome binding. Mol Cell. 2010;40(5):725-35.
20. Krogan NJ, Kim M, Ahn SH, Zhong G, Kobor MS, Cagney G, et al. RNA polymerase II elongation factors of Saccharomyces cerevisiae: a targeted proteomics approach. Mol Cell Biol. 2002;22(20):6979-92.
21. Gavin AC, Bosche M, Krause R, Grandi P, Marzioch M, Bauer A, et al. Functional organization of the yeast proteome by systematic analysis of protein complexes. Nature. 2002;415(6868):141-7.
22. Lindstrom DL, Squazzo SL, Muster N, Burckin TA, Wachter KC, Emigh CA, et al. Dual roles for Spt5 in pre-mRNA processing and transcription elongation revealed by identification of Spt5-associated proteins. Mol Cell Biol. 2003;23(4):1368-78.
23. Reim NI, Chuang J, Jain D, Alver BH, Park PJ, Winston F. The conserved elongation factor Spn1 is required for normal transcription, histone modifications, and splicing in Saccharomyces cerevisiae. Nucleic Acids Res. 2020;48(18):10241-58.
24. Fischbeck JA, Kraemer SM, Stargell LA. SPN1, a conserved gene identified by suppression of a postrecruitment-defective yeast TATA-binding protein mutant. Genetics. 2002;162(4):1605-16.
25. Zhang L, Fletcher AG, Cheung V, Winston F, Stargell LA. Spn1 regulates the recruitment of Spt6 and the Swi/Snf complex during transcriptional activation by RNA polymerase II. Mol Cell Biol. 2008;28(4):1393-403.

26. Cermakova K, Demeulemeester J, Lux V, Nedomova M, Goldman SR, Smith EA, et al. A ubiquitous disordered protein interaction module orchestrates transcription elongation. Science. 2021;374(6571):1113-21.
27. Ramani V, Qiu R, Shendure J. High Sensitivity Profiling of Chromatin Structure by MNase-SSP. Cell Rep. 2019;26(9):2465-76 e4.
28. Brogaard K, Xi L, Wang JP, Widom J. A map of nucleosome positions in yeast at base-pair resolution. Nature. 2012;486(7404):496-501.
29. Thurston AK, Radebaugh CA, Almeida AR, Argueso JL, Stargell LA. Genome Instability Is Promoted by the Chromatin-Binding Protein Spn1 in Saccharomyces cerevisiae. Genetics. 2018;210(4):1227-37.
30. Zhang Z, Reese JC. Isolation of yeast nuclei and micrococcal nuclease mapping of nucleosome positioning. Methods Mol Biol. 2006;313:245-55.
31. Snyder MW, Kircher M, Hill AJ, Daza RM, Shendure J. Cell-free DNA Comprises an In Vivo Nucleosome Footprint that Informs Its Tissues-Of-Origin. Cell. 2016;164(1-2):57-68.
32. Gansauge MT, Meyer M. Single-stranded DNA library preparation for the sequencing of ancient or damaged DNA. Nat Protoc. 2013;8(4):737-48.
33. Martin M. Cutadapt removes adapter sequences from high-throughput sequencing reads. The EMBnet J. 2011;17(3).
34. Langmead B, Salzberg SL. Fast gapped-read alignment with Bowtie 2. Nat Methods. 2012;9(4):357-9.
35. Li H, Handsaker B, Wysoker A, Fennell T, Ruan J, Homer N, et al. The Sequence Alignment/Map format and SAMtools. Bioinformatics. 2009;25(16):2078-9.
36. Quinlan AR, Hall IM. BEDTools: a flexible suite of utilities for comparing genomic features. Bioinformatics. 2010;26(6):841-2.
37. Park D, Morris AR, Battenhouse A, Iyer VR. Simultaneous mapping of transcript ends at single-nucleotide resolution and identification of widespread promoter-associated non-coding RNA governed by TATA elements. Nucleic Acids Res. 2014;42(6):3736-49.
38. Churchman LS, Weissman JS. Nascent transcript sequencing visualizes transcription at nucleotide resolution. Nature. 2011;469(7330):368-73.
39. Chereji RV, Ocampo J, Clark DJ. MNase-Sensitive Complexes in Yeast: Nucleosomes and Non-histone Barriers. Mol Cell. 2017;65(3):565-77 e3.
40. Chereji RV, Ramachandran S, Bryson TD, Henikoff S. Precise genome-wide mapping of single nucleosomes and linkers in vivo. Genome Biol. 2018;19(1):19.
41. Viktorovskaya O, Chuang J, Jain D, Reim NI, Lopez-Rivera F, Murawska M, et al. Essential histone chaperones collaborate to regulate transcription and chromatin integrity. Genes Dev. 2021;35(9-10):698-712.
42. Mayer A, Lidschreiber M, Siebert M, Leike K, Soding J, Cramer P. Uniform transitions of the general RNA polymerase II transcription complex. Nat Struct Mol Biol. 2010;17(10):1272-8.
43. Lorch Y, Maier-Davis B, Kornberg RD. Role of DNA sequence in chromatin remodeling and the formation of nucleosome-free regions. Genes Dev. 2014;28(22):2492-7.
44. Rando OJ, Winston F. Chromatin and transcription in yeast. Genetics. 2012;190(2):351-87.

45. Segal E, Fondufe-Mittendorf Y, Chen L, Thastrom A, Field Y, Moore IK, et al. A genomic code for nucleosome positioning. Nature. 2006;442(7104):772-8.
46. Satchwell SC, Drew HR, Travers AA. Sequence periodicities in chicken nucleosome core DNA. J Mol Biol. 1986;191(4):659-75.
47. Ehara H, Kujirai T, Shirouzu M, Kurumizaka H, Sekine SI. Structural basis of nucleosome disassembly and reassembly by RNAPII elongation complex with FACT. Science. 2022;377(6611):eabp9466.
48. McCullough L, Connell Z, Petersen C, Formosa T. The Abundant Histone Chaperones Spt6 and FACT Collaborate to Assemble, Inspect, and Maintain Chromatin Structure in Saccharomyces cerevisiae. Genetics. 2015;201(3):1031-45.
49. Jeronimo C, Poitras C, Robert F. Histone Recycling by FACT and Spt6 during Transcription Prevents the Scrambling of Histone Modifications. Cell Rep. 2019;28(5):1206-18 e8.
50. Uzun U, Brown T, Fischl H, Angel A, Mellor J. Spt4 facilitates the movement of RNA polymerase II through the +2 nucleosomal barrier. Cell Rep. 2021;36(13):109755.
51. Doris SM, Chuang J, Viktorovskaya O, Murawska M, Spatt D, Churchman LS, Winston F. Spt6 Is Required for the Fidelity of Promoter Selection. Mol Cell. 2018;72(4):687-99 e6.
52. van Bakel H, Tsui K, Gebbia M, Mnaimneh S, Hughes TR, Nislow C. A compendium of nucleosome and transcript profiles reveals determinants of chromatin architecture and transcription. PLoS Genet. 2013;9(5):e1003479.
53. Tramantano M, Sun L, Au C, Labuz D, Liu Z, Chou M, et al. Constitutive turnover of histone H2A.Z at yeast promoters requires the preinitiation complex. Elife. 2016;5.
54. Feng J, Gan H, Eaton ML, Zhou H, Li S, Belsky JA, et al. Noncoding Transcription Is a Driving Force for Nucleosome Instability in spt16 Mutant Cells. Mol Cell Biol. 2016;36(13):1856-67.

TABLE AND FIGURES LEGENDS

Figure 1. An extensive characterization of MNase produced fragments suggests shifts in chromatin protections in Spn1 mutant yeast across fragment lengths. (A) Nuclei harvested from two biological replicates of wild-type and mutant Spn1 expressing yeast grown to log phase were digested with 128U MNase and protected fragments were isolated and sequenced. V-plots were produced by mapping fragment midpoints ~30-180 bp in length to the yeast genome anchored at +1, +2, and +5 nucleosome dyad positions from 4688 genes. (B) Difference V-plots produced by quantifying differences between wild-type and *spn1*^{K192N} (left hand panels) and *spn1*$^{141-305}$ (right hand panels) fragment midpoint occupancies in (A). Regions in red come from an increase in fragment density in the mutant Spn1 expressing yeast while regions in blue come from a decrease in fragment density in the mutant Spn1 expressing yeast. The box over the *spn1*^{K192N} difference V-plot highlights a reduction in protection over NDRs while the box over the *spn1*$^{141-305}$ difference plot highlights the shift in chromatin protections.

Figure 2. Mutations in Spn1 produce a downstream shift in nucleosome positioning over open reading frames genome wide. (A) Difference heatmap between wild-type and mutant Spn1 expressing yeast strains scored by changes in nucleosome occupancy. Genes are aligned by their +1 nucleosome dyad position and ranked by length. Scores are calculated by subtracting wild-type nucleosome occupancy data from mutant nucleosome occupancy. Regions in red are enriched for nucleosomes at that position while blue regions are depleted for nucleosomes. (B) Profiles of MNase protected fragments (80-170 bp) mapped over 4688 genes aligned to the +1 nucleosome dyad in wild-type, *spn1*^{K192N}, and *spn1*$^{141-305}$ expressing yeast. (C) Difference profile plot between wild-type and mutant samples. Average nucleosome density from wild-type expressing yeast is plotted in grey. Differences between wild-type and mutants (*spn1*^{K192N}, red and *spn1*$^{141-305}$, blue) against wild-type replicates are plotted. (D) Difference profile plots between wild-type and mutant samples over 4688 genes binned into quartiles by published NET-seq data (38), with Q1 representing the lowest levels of Rpb3 (left panel) and Q4 representing the highest (right panel). (E) Difference profile plots between wild-type and mutant

samples over 4688 genes binned into quartiles by length, with Q1 representing the shortest genes (left panel), and Q4 representing the longest genes (right panel).

Figure 3. The *spn1^{K192N}* mutation reduces the stability of nucleosome-depleted regions. (A) Profiles of MNase protected fragments (0-60 bp) mapped over 4688 genes aligned to the +1 nucleosome dyad in wild-type, *spn1^{K192N}*, and *spn1$^{141-305}$* expressing yeast. (B) Profiles of MNase protected fragments (61-71 bp) mapped over 4688 genes aligned to the +1 nucleosome dyad in wild-type, *spn1^{K192N}*, and *spn1$^{141-305}$* expressing yeast. (C) Profiles of MNase protected fragments (0-60 bp) from low MNase-digested samples (32U) mapped over 4688 genes aligned to the +1 nucleosome dyad in wild-type, *spn1^{K192N}*, and *spn1$^{141-305}$* expressing yeast. (D) Profiles of MNase protected fragments (61-71 bp) from low MNase-digested samples (32U) mapped over 4688 genes aligned to the +1 nucleosome dyad in wild-type, *spn1^{K192N}*, and *spn1$^{141-305}$* expressing yeast.

Figure 4. Quantification of nucleosome positioning shifts in Spn1-mutant cells reveals that nucleosomes are redistributed at rotational positions. (A) Metagene plots of fragment midpoints 142-152 bp in length mapped to the +5 nucleosome dyad at gene quartiles ranked by expression. (B) Metagene plots of fragment midpoints 142-152 bp in length mapped to the +5 nucleosome dyad at gene quartiles ranked by length. (C) Difference heatmaps between wild-type and mutant Spn1 expressing yeast strains scored by changes in occupancy at rotational positions surrounding each nucleosome dyad position at genes ranked by published NET-seq data (38). (D) Difference heatmaps between wild-type and mutant Spn1 expressing yeast strains scored by changes in occupancy at rotational positions surrounding each nucleosome dyad position at genes ranked by length.

Figure 5. Mutations in Spn1 produce a downstream shift in hexasome positioning over open reading frames genome wide. (A) Metagene plots of fragment midpoints 102-112 bp in

length mapped to the +5 nucleosome dyad at gene quartiles ranked by expression. (B) Metagene plots of fragment midpoints 102-112 bp in length mapped to the +5 nucleosome dyad at gene quartiles ranked by length. (C) Difference heatmaps between wild-type and mutant Spn1 expressing yeast strains scored by changes in occupancy at rotational positions surrounding each nucleosome dyad position at genes ranked by published NET-seq data (38). (D) Difference heatmaps between wild-type and mutant Spn1 expressing yeast strains scored by changes in occupancy at rotational positions surrounding each nucleosome dyad position at genes ranked by length.

Figure 6. Mutations in Spn1 produce slight perturbations in tetrasome positioning over open reading frames genome wide. (A) Metagene plots of fragment midpoints 61-71 bp in length mapped to the +5 nucleosome dyad at gene quartiles ranked by expression. (B) Metagene plots of fragment midpoints 61-71 bp in length mapped to the +5 nucleosome dyad at gene quartiles ranked by length. (C) Difference heatmaps between wild-type and mutant Spn1 expressing yeast strains scored by changes in occupancy at rotational positions surrounding each nucleosome dyad position at genes ranked by published NET-seq data (38). (D) Difference heatmaps between wild-type and mutant Spn1 expressing yeast strains scored by changes in occupancy at rotational positions surrounding each nucleosome dyad position at genes ranked by length.

Figure 1

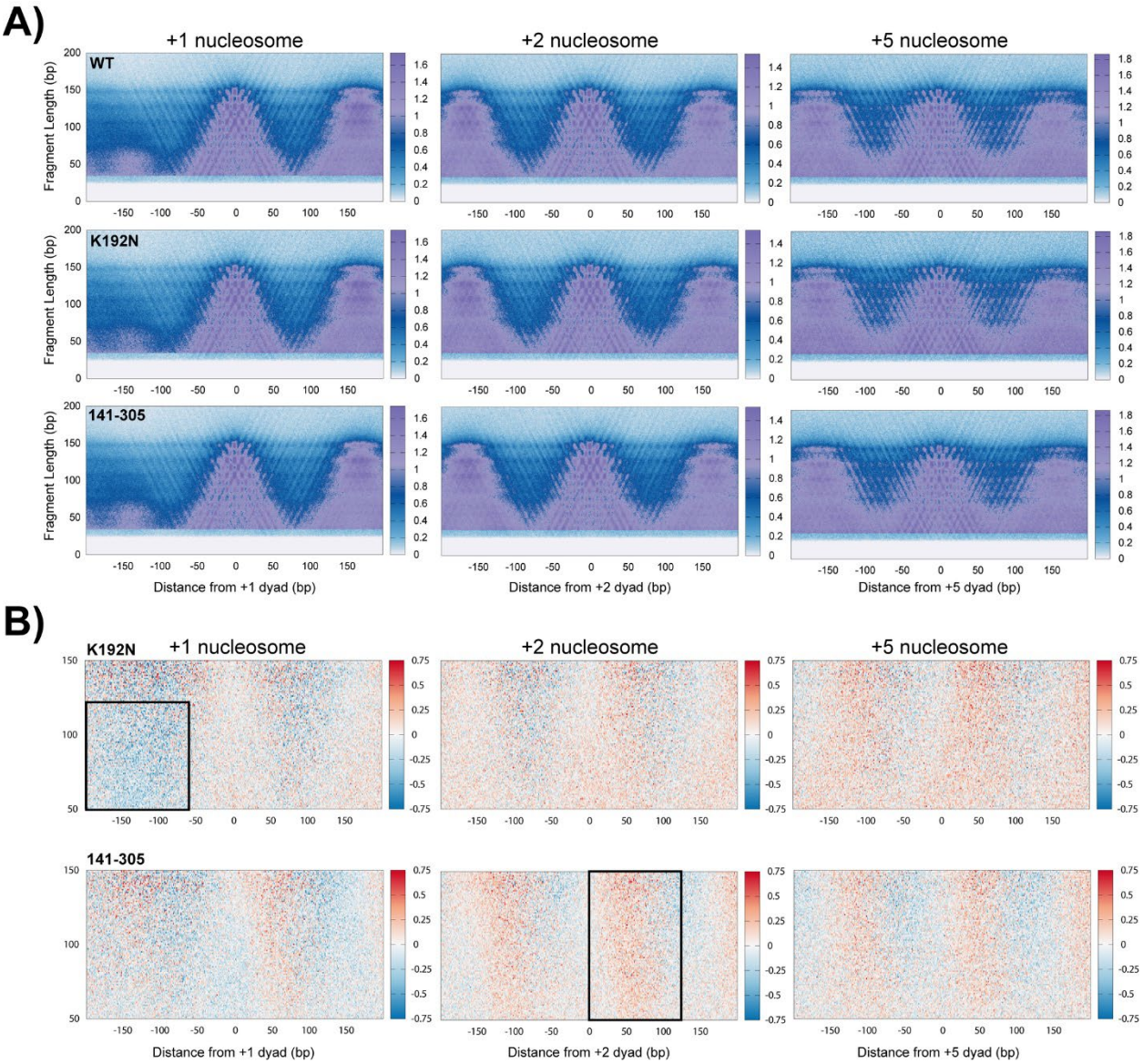
A)
+1 nucleosome
+2 nucleosome
+5 nucleosome
WT
K192N
141-305
Fragment Length (bp)
Distance from +1 dyad (bp)
Distance from +2 dyad (bp)
Distance from +5 dyad (bp)
B)
K192N
141-305

Figure 2

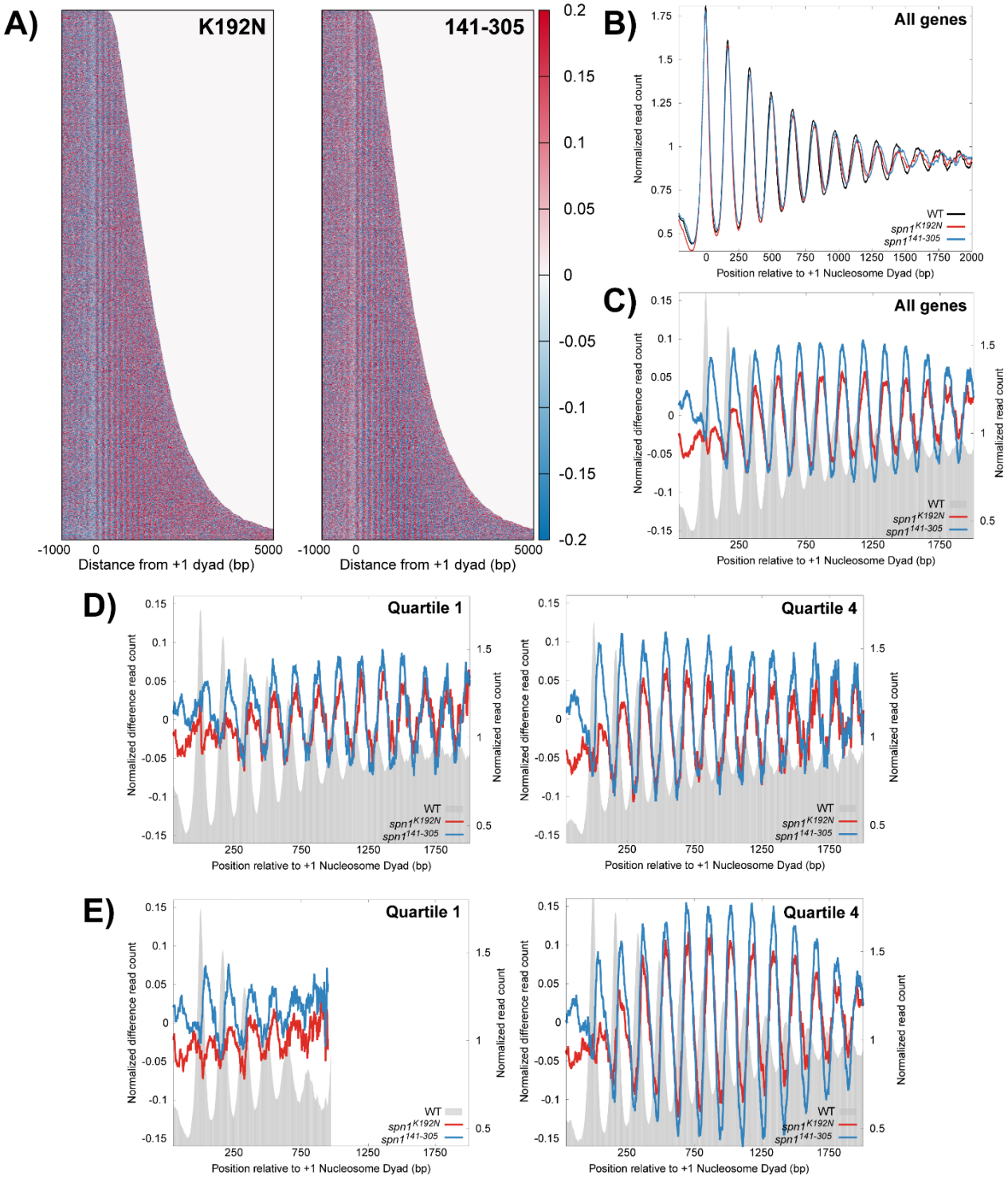
A)
K192N
141-305
-1000
0
5000
Distance from +1 dyad (bp)
0.2
0.15
0.1
0.05
0
-0.05
-0.1
-0.15
-0.2
B)
All genes
Normalized read count
Position relative to +1 Nucleosome Dyad (bp)
WT
spn1K192N
spn1141-305
C)
All genes
Normalized difference read count
Normalized read count
D)
Quartile 1
Quartile 4
E)
Quartile 1
Quartile 4

Figure 3

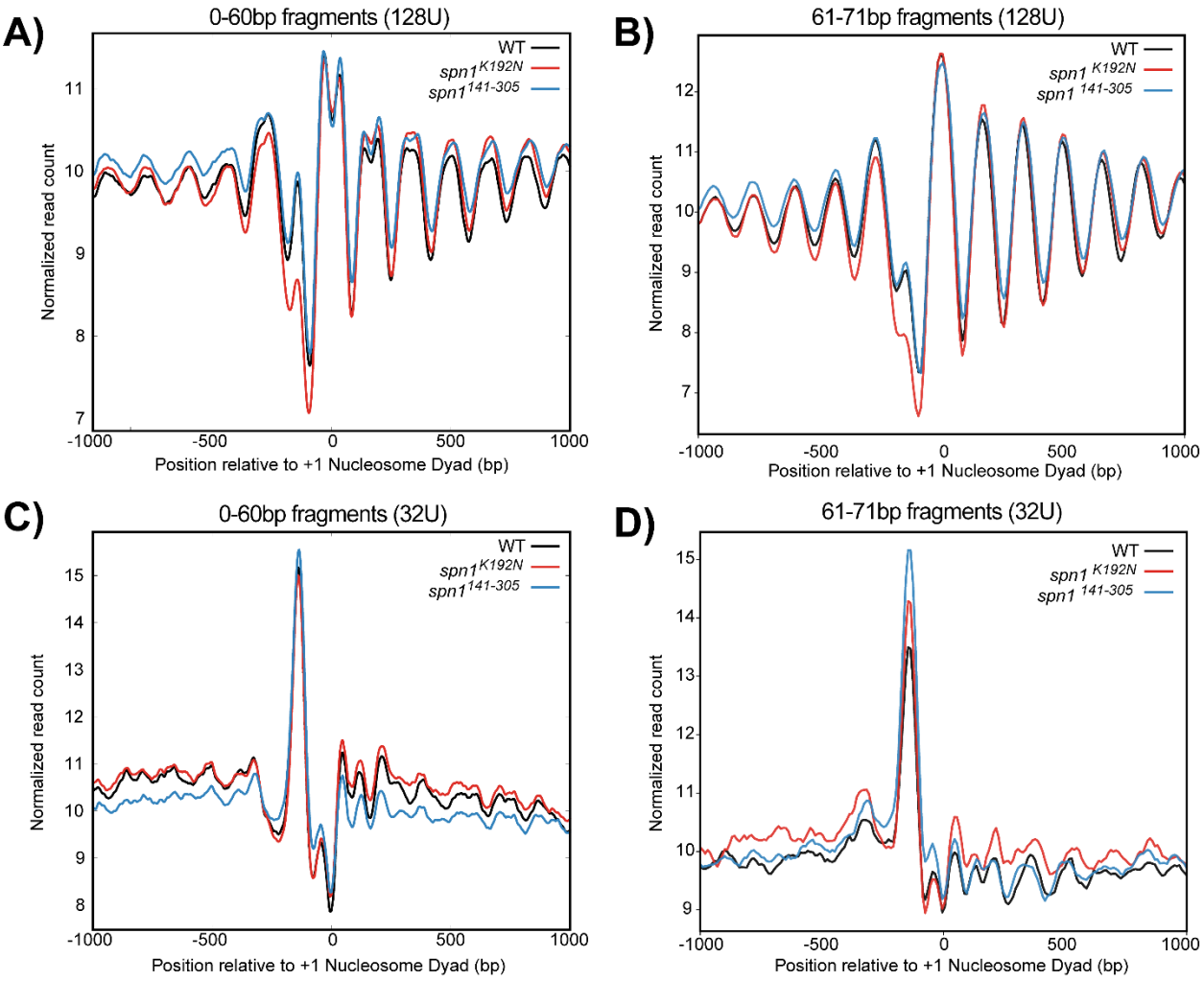
A)
0-60bp fragments (128U)
WT
spn1 K192N
spn1 141-305
Normalized read count
Position relative to +1 Nucleosome Dyad (bp)
B)
61-71bp fragments (128U)
WT
spn1 K192N
spn1 141-305
Normalized read count
Position relative to +1 Nucleosome Dyad (bp)
C)
0-60bp fragments (32U)
WT
spn1 K192N
spn1 141-305
Normalized read count
Position relative to +1 Nucleosome Dyad (bp)
D)
61-71bp fragments (32U)
WT
spn1 K192N
spn1 141-305
Normalized read count
Position relative to +1 Nucleosome Dyad (bp)

Figure 4

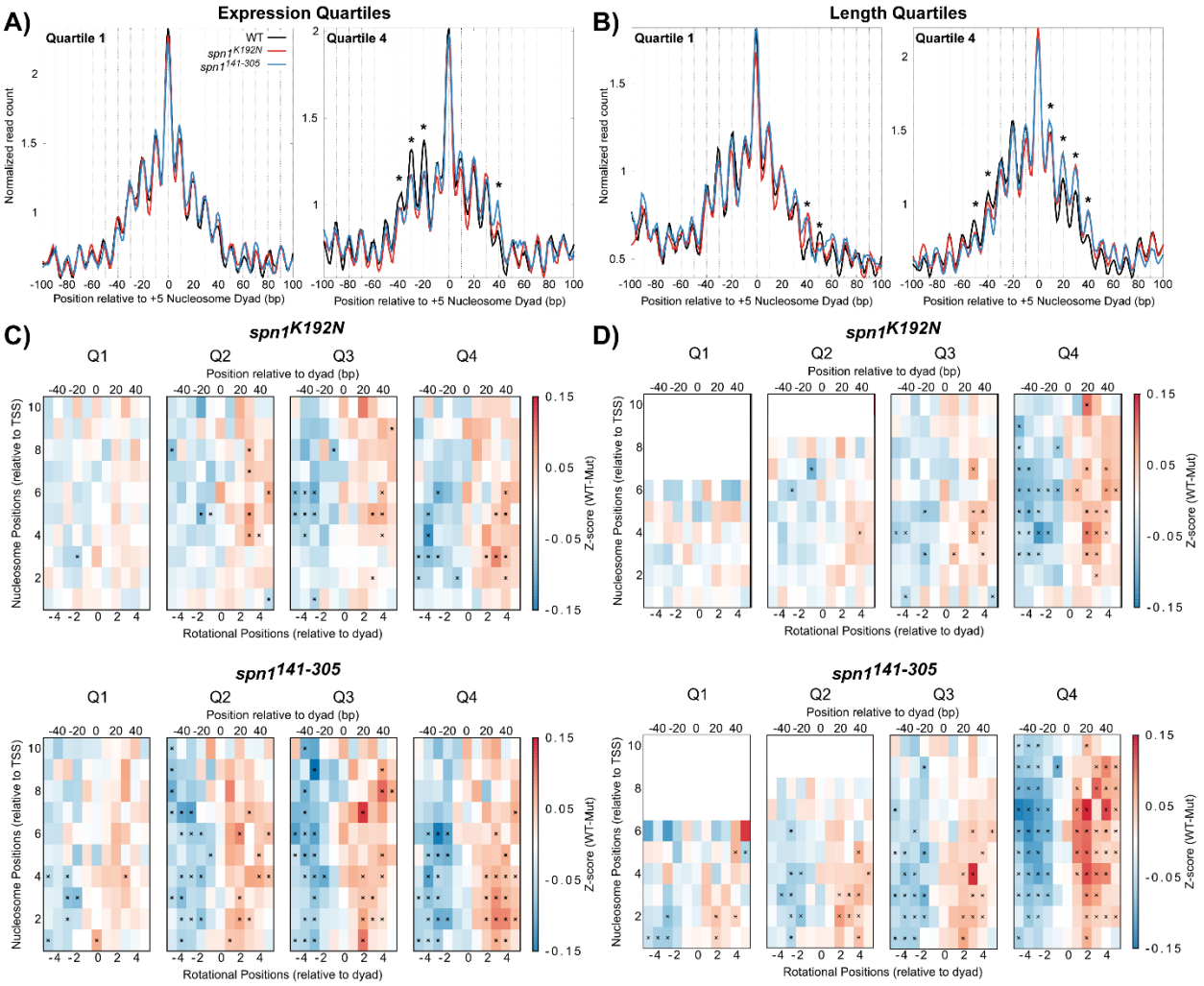
A)
Expression Quartiles
Quartile 1
Quartile 4
WT
spn1K192N
spn1141-305
Normalized read count
Position relative to +5 Nucleosome Dyad (bp)
B)
Length Quartiles
Quartile 1
Quartile 4
Normalized read count
Position relative to +5 Nucleosome Dyad (bp)
C)
spn1K192N
Q1
Q2
Q3
Q4
Position relative to dyad (bp)
Nucleosome Positions (relative to TSS)
Rotational Positions (relative to dyad)
Z-score (WT-Mut)
D)
spn1K192N
spn1141-305
Position relative to dyad (bp)
Nucleosome Positions (relative to TSS)
Rotational Positions (relative to dyad)
Z-score (WT-Mut)

Figure 5

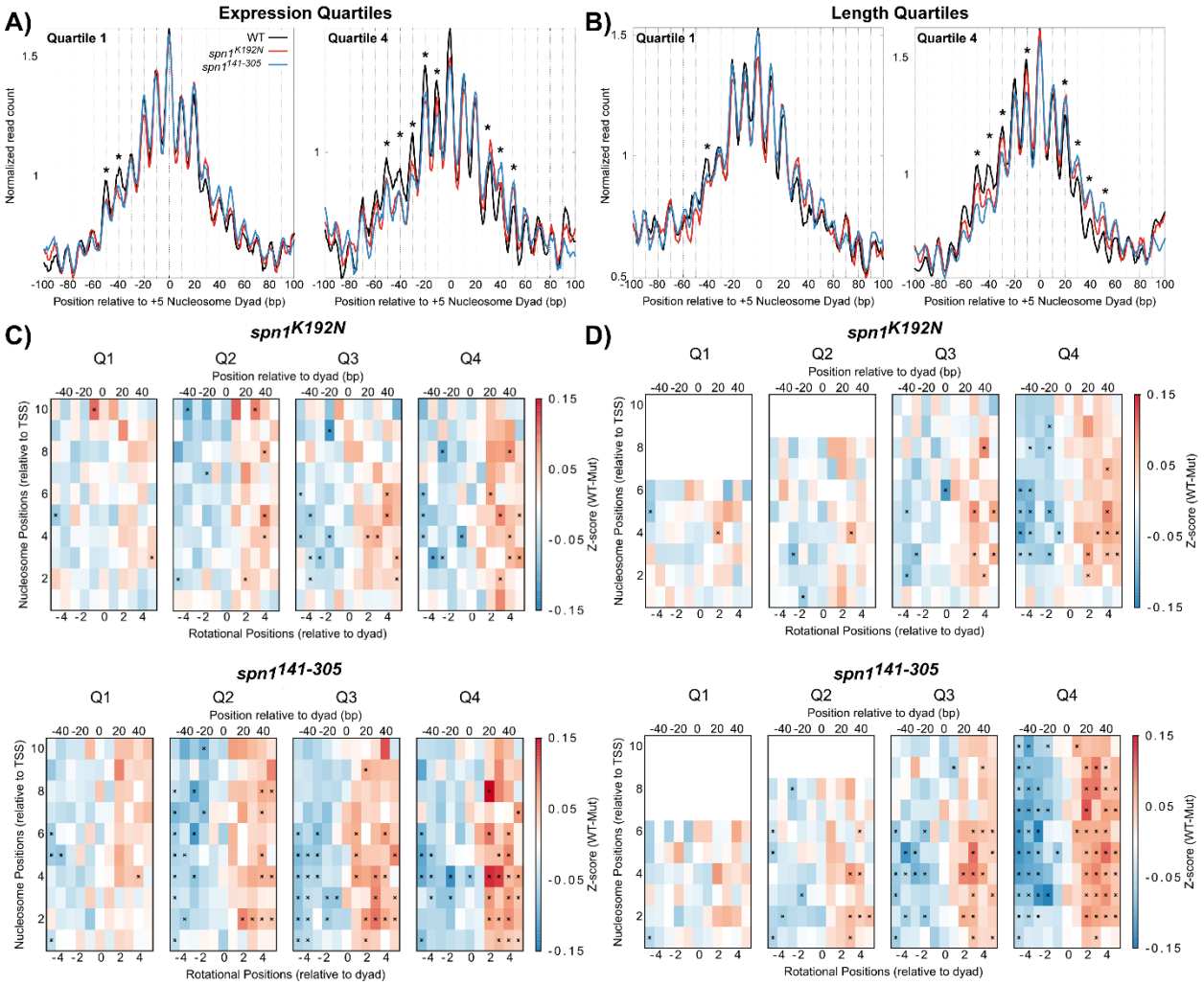
A)
Expression Quartiles
Quartile 1
Quartile 4
WT
spn1K192N
spn1141-305
Normalized read count
Position relative to +5 Nucleosome Dyad (bp)
B)
Length Quartiles
Quartile 1
Quartile 4
Normalized read count
Position relative to +5 Nucleosome Dyad (bp)
C)
spn1K192N
Q1
Q2
Q3
Q4
Position relative to dyad (bp)
Nucleosome Positions (relative to TSS)
Rotational Positions (relative to dyad)
Z-score (WT-Mut)
D)
spn1K192N
Q1
Q2
Q3
Q4
Position relative to dyad (bp)
Nucleosome Positions (relative to TSS)
Rotational Positions (relative to dyad)
Z-score (WT-Mut)
spn1141-305
Q1
Q2
Q3
Q4
Position relative to dyad (bp)
Nucleosome Positions (relative to TSS)
Rotational Positions (relative to dyad)
Z-score (WT-Mut)
spn1141-305
Q1
Q2
Q3
Q4
Position relative to dyad (bp)
Nucleosome Positions (relative to TSS)
Rotational Positions (relative to dyad)
Z-score (WT-Mut)

Figure 6

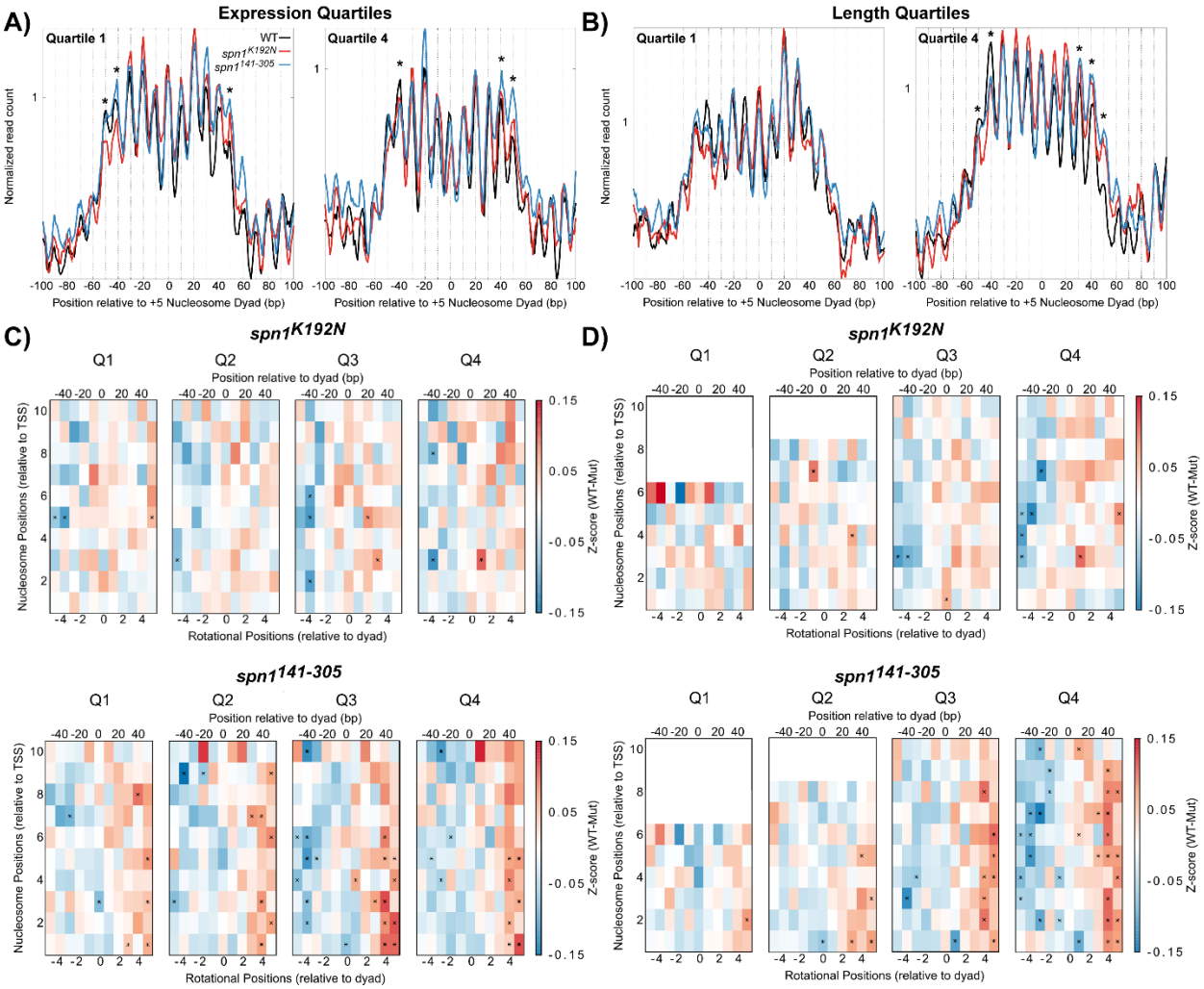
A)
Expression Quartiles
Quartile 1
Quartile 4
WT
spn1K192N
spn1141-305
Normalized read count
Position relative to +5 Nucleosome Dyad (bp)
B)
Length Quartiles
Quartile 1
Quartile 4
Normalized read count
Position relative to +5 Nucleosome Dyad (bp)
C)
spn1K192N
Q1
Q2
Q3
Q4
Position relative to dyad (bp)
Nucleosome Positions (relative to TSS)
Rotational Positions (relative to dyad)
Z-score (WT-Mut)
D)
spn1K192N
Q1
Q2
Q3
Q4
Position relative to dyad (bp)
Nucleosome Positions (relative to TSS)
Rotational Positions (relative to dyad)
Z-score (WT-Mut)
spn1141-305
Q1
Q2
Q3
Q4
Position relative to dyad (bp)
Nucleosome Positions (relative to TSS)
Rotational Positions (relative to dyad)
Z-score (WT-Mut)
spn1141-305
Q1
Q2
Q3
Q4
Position relative to dyad (bp)
Nucleosome Positions (relative to TSS)
Rotational Positions (relative to dyad)
Z-score (WT-Mut)